Dynamics of Wound Closure in Living Nematic Epithelia

Henry Andralojc,[1,*] Jake Turley,[1,2,3] Helen Weavers,[3] Paul Martin,[3] Isaac V. Chenchiah,[1] Rachel R. Bennett,[1,4,†] and Tanniemola B. Liverpool[1,4,‡]

[1]School of Mathematics, University of Bristol, Fry Building, Woodland Road, Bristol BS8 1UG, United Kingdom
[2]Mechanobiology Institute, National University of Singapore, Singapore, Singapore
[3]School of Biochemistry, University of Bristol, University Walk, Bristol BS8 1TD, United Kingdom
[4]Isaac Newton Institute for Mathematical Sciences, 20 Clarkson Road, Cambridge CB3 0EH, United Kingdom

(Received 12 June 2025; accepted 13 February 2026; published 16 April 2026)

We study theoretically the closure of a wound in a layer of epithelial cells in a living tissue after damage. Our analysis is informed by our recent experiments observing reepithelialization *in vivo* of *Drosophila* pupae. On time and length scales such that the evolution of the epithelial tissue near the wound is well captured by that of a 2D active fluid with local nematic order, we consider the free-surface problem of a hole in a bounded region of tissue, and study the role that active stresses in the surrounding tissue play in the closure of the hole. For parallel anchored nematic order at the wound boundary (as we observe in our experiments), we find that closure is accelerated by contractile active stresses and is slowed down when the stresses are extensile. Parallel anchoring also leads to the appearance of topological defects that annihilate upon wound closure.

DOI: 10.1103/8871-8m6c

Tissue damage triggers a complex series of overlapping cell and tissue movements that are reminiscent of many of the processes found in embryonic morphogenesis [1]. These processes together stave off infection and eventually repair the wound, bringing the tissue back to something approaching its prewounded state [2–6]. A key stage of wound healing is reepithelialization, in which the epidermal cells at the cut wound edge and the sheet of epithelium behind them advance to seal the wound gap. Individual and concerted cell contractions and *shape changes*, as well as cell *movements* and/or migration and cell *divisions*, all contribute to the closure of the epithelial gap [7–12]. However precisely how much each of these different cell behaviors, and the forces associated with them, contributes to the ultimate wound healing goal is not known. This is because tissues in many organisms are opaque, and hence it is difficult to quantify the contribution of these processes. Therefore the study of translucent tissue from genetically tractable organisms like *Drosophila melanogaster* [9,13–18] can play a valuable role in leading us toward the required mechanistic understanding of the process [19–21]. The hope is that studying the cellular responses to wounding in such model systems can give insight into mammalian healing, ultimately leading to the development of practices that can aid clinicians and patients [5,22]. Such studies can also inspire design principles for developing self-healing artificial systems.

Mechanical models for reepithelialization typically consider the surrounding tissue to be an isotropic passive medium where closure is driven by cell proliferation [23,24] or *two* actin-based machineries localized at the wound edge [23,25–31], possibly coupled to chemical signals [32]. These are (1) the actin "purse string" [13,33–36] (a bundle of filaments at the wound edge that constricts, dragging the surrounding tissue radially inward) and (2) filopodia or lamellipodia (motile extrusions from the leading edge cells that extend into the wound space and drag the cells behind [37]), both of which are active *boundary* conditions at the wound edge. There is increasing evidence, however, that cells far from the wound play a role in the closure of the epithelial gap [7,9,10,38–41]. Hence, here we present a general continuum framework for reepithelialization that includes *active* forces in the *bulk* tissue [10,37,42–46], inspired by our recent experiments [11,47–49].

In these experiments on the *Drosophila* pupa wing epithelium [11,47–49], an approximately circular wound was followed using time-lapse confocal microscopy. Cell shapes, motion, and divisions were tracked and classified using fluorescent tagging and machine learning [48]. We observed that (1) in unwounded tissue, the typical cell is elongated, head-tail symmetric, and aligned along the long axis of the wing (i.e., with nematic symmetry); (2) cells

*Contact author: h.andralojc@bristol.ac.uk
†Contact author: rachel.bennett@bristol.ac.uk
‡Contact author: t.liverpool@bristol.ac.uk

Published by the American Physical Society under the terms of the Creative Commons Attribution 4.0 International license. Further distribution of this work must maintain attribution to the author(s) and the published article's title, journal citation, and DOI.

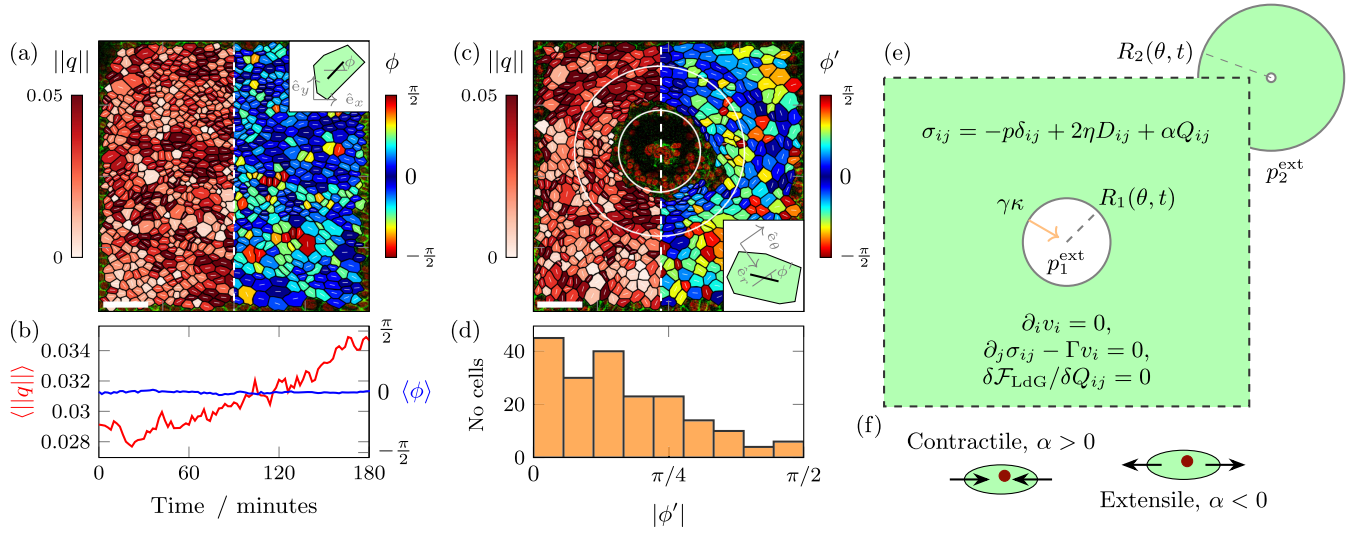


FIG. 1. (a) Time-lapse movies of the developing *Drosophila* pupal epithelium (18 h after puparium formation) show unwounded tissue has nematic order. Elongation and alignment of each epithelial cell is described by a traceless shape tensor, q, its magnitude $\|q\| = \frac{1}{2}\mathrm{Tr}(q^2)$ gives shape anisotropy and $\phi \in [-\pi/2, \pi/2)$ gives the direction of nematic alignment relative to the x axis. (b) Epithelial cells align, on average, along the proximodistal axis of the wing (roughly aligning with the x axis), the degree of elongation increasing as the tissue develops. (c) Snapshot of tissue ~8 min postwounding. Cellular alignment, ϕ', is measured relative to the radial direction in a polar basis centered on the wound as illustrated in the inset: red (blue) cells indicate alignment along $\pm\hat{\mathbf{e}}_\theta$ ($\pm\hat{\mathbf{e}}_r$). (d) Distribution of $|\phi'|$'s for cells inside annulus illustrated in panel (c). We find that cells close to the wound initially tend to be aligned along the $\pm\hat{\mathbf{e}}_\theta$ direction. (e) Illustration of the model setup and (f) the active contractile and extensile force dipoles included in the model that coarse-grain to generate a stress $\sim\alpha\mathbf{Q}$.

close to the wound edge are aligned tangential to the wound edge rather than the bulk tissue (wing axis) [11,48]; and (3) there was a dramatic decrease in the division rate near a wound [11,48] during gap closure, i.e., the tissue is approximately incompressible [26].

We thus model the wounded epithelium as a two-dimensional active nematic [50–53] with a hole at its center with parallel anchoring at the wound edge. On the timescale of healing [11], the tissue flows like an incompressible viscous fluid. Using this, we show how activity of the bulk tissue modulates wound closure, finding that, for parallel-anchored nematic boundary conditions, contractile active stresses accelerate wound closure while extensile active stresses delay it. Our analysis predicts that initially circular wounds become anisotropic as the wound closes, which we verify from experiment. Interestingly, parallel anchoring requires two $-\frac{1}{2}$ topological defects [54–58] that, together with the wound hole (topological charge $+1$), annihilate upon closure, leaving an "unscarred" epithelium with no memory of the wound.

From experiment to model—Following segmentation of experimental videos, the cell and wound boundaries are identified and approximated by polygons. Moments over each polygon's interior quantify the locations, areas, and shapes of the polygon in each time-lapse frame. Of particular interest to us is the traceless shape tensor, q, quantifying elongation and alignment of a polygon,

$$q = \frac{1}{A^2}\int_{\text{poly}} \mathrm{d}x\mathrm{d}y \begin{pmatrix} x^2 - y^2 & xy \\ xy & y^2 - x^2 \end{pmatrix}, \tag{1}$$

where the integral is over the polygon's interior and A, the area of the polygon in question. Like the rank-2 nematic order parameter [59], q may be written in terms of alignments along a basis set, e.g., $q = \begin{pmatrix} q_{xx} & q_{xy} \\ q_{xy} & -q_{xx} \end{pmatrix}$, or in terms of a magnitude and angle $q = \|q\| \begin{pmatrix} \cos 2\phi & \sin 2\phi \\ \sin 2\phi & -\cos 2\phi \end{pmatrix}$, where the magnitude $\|q\| = \frac{1}{2}\mathrm{Tr}(q^2) = q_{xx}^2 + q_{xy}^2$ gives a measure for the degree of elongation of each polygon ($\|q\| = 0$ for isotropic polygons, $\|q\| \neq 0$ for anisotropic polygons), and the angle, defined as $\tan 2\phi = (q_{xy}/q_{xx})$ defines the axis of alignment for the polygon relative to the x axis. We will use $\|q\|$ as a measure for anisotropy in both cell and wound shapes.

Figure 1(a) illustrates a snapshot of the segmented cells in an unwounded sample, color coded by magnitude of $\|q\|$ and angle relative to the x axis in each half. Averaging over all cells in each frame [Fig. 1(b)], we find that the typical cell elongates along the proximodistal axis of the developing wing (which aligns with the x axis of our imaging setup) showing the tissue has nematic symmetry. We note that by rotating each cell's q into a polar basis centered on the wound [see Supplemental Material (SM) [60]], we find that the cells close to a wound tend to align not along the bulk tissue axis but parallel to the wound edge [Figs. 1(c) and 1(d)].

Taking the continuum limit, local cell shape anisotropy is described by the traceless symmetric 2×2 tensor field, $\mathbf{Q}(\mathbf{r}, t)$ [59,61], and motion by an incompressible velocity field, $\mathbf{v}(\mathbf{r}, t)$, and an associated pressure, $p(\mathbf{r}, t)$. We study the time evolution of these fields in a bounded domain following the removal of a circular disk from its center at $t = 0$, with parallel anchoring for $\mathbf{Q}$ at the wound edge and x-axis alignment in the far field, using active nematohydrodynamics at vanishing Reynolds number in contact with a frictional substrate [51,53,62,63],

$$0 = \nabla \cdot \mathbf{v}, \tag{2a}$$

$$0 = -\nabla p + \eta \nabla^2 \mathbf{v} - \Gamma \mathbf{v} + \alpha \nabla \cdot \mathbf{Q}, \tag{2b}$$

$$0 = \frac{\delta \mathcal{F}_{\mathrm{LdG}}}{\delta \mathbf{Q}}, \tag{2c}$$

where $\mathcal{F}_{\mathrm{LdG}}$ is a Landau–de Gennes free energy [53,59],

$$\mathcal{F}_{\mathrm{LdG}} = \int \mathrm{d}x \left[-\frac{A}{2} \|\mathbf{Q}\|^2 + \frac{B}{4} \|\mathbf{Q}\|^4 + \frac{K}{2} \|\nabla \mathbf{Q}\|^2 \right], \tag{3}$$

with $\|\mathbf{Q}\|^2 = Q_{ij} Q_{ij}$, $\|\nabla \mathbf{Q}\|^2 = \partial_i Q_{jk} \partial_i Q_{jk}$. η is the bulk viscosity and Γ is the friction coefficient, which we include to model the effect of a basal membrane or cuticle resisting the flow of the tissue above or below it. The active stress $\sigma^a_{ij} = \alpha Q_{ij}$ is present when $\alpha \neq 0$ [53,64]. We have assumed that $\mathbf{Q}$ relaxes much faster than $\mathbf{v}$, so the nematic texture is always in a local equilibrium. We consider the wound sufficiently far from the outer wing boundary that it does not affect the wound and choose, for simplicity, an initially circular outer boundary [see Fig. 1(e)]. We also ignore elastic contributions to the fluid stress arising due to variations in $\mathbf{Q}$ as they are higher order in gradient and subdominant at long length scales [53].

We solve these subject to standard kinematic and dynamic boundary conditions on each free surface, labeled by $r = |\mathbf{r}| = R_i(\theta, t)$ for $i = 1, 2$ for the inner and outer free surfaces, respectively (θ is the polar angle), in addition to conditions on the components of $\mathbf{Q}$ [see Eq. (S15) [60]]. The dynamic boundary condition imposes force balance on every point on the free boundary,

$$[(p_i^{\mathrm{ext}} - p)\mathbf{n} + (2\eta \mathbf{D} + \alpha \mathbf{Q}) \cdot \mathbf{n}]|_{R_i} = \gamma \kappa_i \mathbf{n}, \tag{4}$$

where p_i^{ext} is the pressure of the exterior fluid in contact with the ith free surface, $D_{jk} = \frac{1}{2}(\partial_j v_k + \partial_k v_j)$ is the rate of strain tensor [65], $\mathbf{n}$ is the unit normal to the boundary, and κ_i is the local curvature of the ith surface. The effective surface tension $\gamma = \tilde{\gamma} + \tau > 0$ contains both a constant passive surface tension $\tilde{\gamma}$ and an active term τ, which we include to model the possible presence of a constricting actin purse string, (see SM [60] for details). The kinematic boundary condition then governs the time evolution of the free surfaces, requiring that the flow convects the boundary,

$$D_t[r - R_i(\theta, t)] = 0 \Rightarrow v_r|_{R_i} = \dot{R}_i + \frac{v_\theta|_{R_i}}{R_i} R_i', \tag{5}$$

where $D_t = \partial_t + \mathbf{v} \cdot \nabla$ is the Lagrangian material derivative.

We nondimensionalize our equations: $\mathbf{r} \to L\mathbf{r}$, $t \to Tt$, $p \to \Pi p$, $\mathbf{Q} \to Q_0 \mathbf{Q}$, choosing $L = \sqrt{\eta/\Gamma}$, $T = \eta/\Pi$, $\Pi = \gamma/L$, $Q_0 = \sqrt{A/2B}$, and define nondimensional parameters $\epsilon_\alpha = \alpha Q_0/\Pi$ (relative importance of active to other stresses), and $\Lambda = L/\ell_Q$ (relative sizes of the flow and nematic relaxation length, $\ell_Q^2 = K/2A$, scales). $1/\Lambda$ controls the nematic length scale, and thus the persistence of active forces into the bulk of the fluid.

The wounds in our experiments are initially approximately circular [49]. Therefore, we solve Eq. (2) by expanding the dynamical fields in the activity, ϵ_α,

$$R_i(\theta, t) = R_i^0(t) + \epsilon_\alpha R_i^1(\theta, t), \tag{6a}$$

$$\mathbf{v}(r, \theta, t) = \mathbf{v}^0(r, t) + \epsilon_\alpha \mathbf{v}^1(r, \theta, t) + \cdots, \tag{6b}$$

$$p = p^0 + \epsilon_\alpha p^1 + \cdots, \tag{6c}$$

$$\mathbf{Q} = \mathbf{Q}^0 + \epsilon_\alpha \mathbf{Q}^1 + \cdots, \tag{6d}$$

and decomposing into Fourier modes [66],

$$R_i^1(\theta, t) = \sum_{n=0}^{\infty} \xi_i^n(t) \cos n\theta + \eta_i^n(t) \sin n\theta, \tag{7}$$

so the leading-order problem is a droplet of passive viscous fluid with a circular hole at the center, whose closure is driven by an (active) surface tension and differences in external pressures. The flow at first order in activity is additionally driven by leading-order gradients in $\mathbf{Q}$, i.e., the nematic response to a circular boundary. The magnitude of the active stress in tissue typically cannot be measured directly, and so we cannot confidently claim that ϵ_α is a small parameter, however the fact that the wounds inflicted are initially of circular cross section suggest it is *a posteriori*, $\epsilon_\alpha R_i^1/R_i^0 \ll 1$, for short times. The continuum approach will also of course break down as the wound size approaches the typical cell size and the division rate returns to levels observed in healthy tissue. Therefore, although we solve the equations of motion up to closure, we shall mainly focus on short times following wounding.

Passive bulk tissue with active hole—The flow at leading order is radial by symmetry and independent of $\mathbf{Q}$. Solving for p^0, $\mathbf{v}^0$ (see SM [60]), we substitute into the kinematic boundary condition to obtain an ordinary differential equation (ODE) for the inner mode radius (momentarily reinstating dimensional quantities),

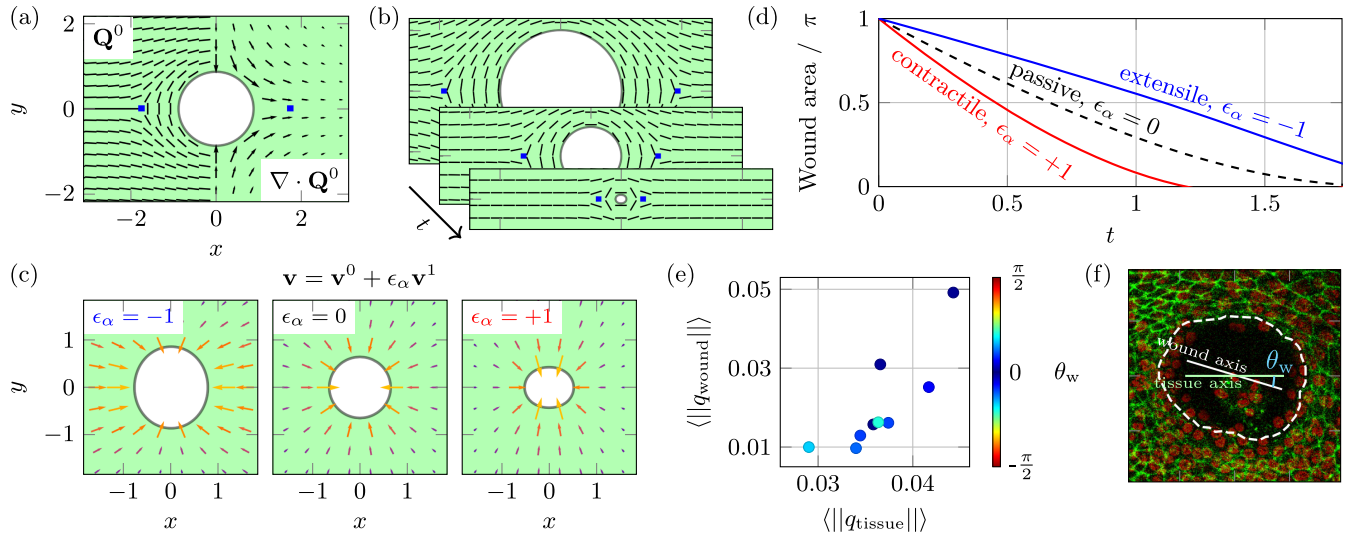


FIG. 2. (a) Nematic texture (left) and active force (right) that drives the flow. The blue squares mark positions of $-\frac{1}{2}$ topological defects. (b) Snapshots of nematic texture throughout closure show the motion of defects toward the origin, resulting in a topologically "healed" final state. (c) Flow surrounding wound boundary for identical initial conditions but varying values of ϵ_α. (d) Wound areas throughout closure for different values of ϵ_α. Panels (a)–(d) plotted with $\Lambda = 0.1$, $R_1^0(0) = 0$, $R_2^0(0) = 20$. (e) Experimental observation of correlation between wound anisotropy and degree of nematic order in the surrounding epithelium. $\langle ||q_{\ldots}|| \rangle$ corresponds to average magnitude of q tensor for cells or wounds, averaging over all cells or wounds in first ~10 min (5 frames) of each time lapse. Points are different wounds, with color indicating value of θ_w—illustrated in (f)—the angle between the tissue axis and the major axis of the wound polygon averaged over initial ~10 min.

$$\dot{R}_1^0 = -\frac{\gamma R_2^0(R_2^0 + R_1^0) + P R_1^0 (R_2^0)^2}{2\eta[(R_2^0)^2 - (R_1^0)^2] + \Gamma (R_1^0 R_2^0)^2 \log \frac{R_2^0}{R_1^0}}, \tag{8}$$

where P is the difference in external pressures at the inner and outer boundaries, $P = p_2^{\text{ext}} - p_1^{\text{ext}}$. We see that, at leading order, closure is driven by the effective surface tension (which includes both passive surface tension and active purse-string contributions) and positive pressure differences ($P > 0$) and is slowed by (dissipative) viscosity, friction, and negative pressure differences ($P < 0$).

Nematic texture and active stresses—When we switch on activity ($\alpha \neq 0$), the shape anisotropy, $\mathbf{Q}$, becomes relevant, generating a nematic texture between the inner and outer radii, $R_1^0(t), R_2^0(t)$. Minimization of free energy in Eq. (3) results in a nonlinear partial differential equation, which we linearize by expanding around the homogeneous ordered state, aligning with the x axis, $Q_{xx}^0 = 1 + q_1$, $Q_{xy}^0 = q_2$, to obtain $\nabla^2 q_1 - \Lambda^2 q_1 \approx 0$, $\nabla^2 q_2 \approx 0$, a good approximation provided $|q_1|, |q_2| \ll 1$. We take parallel anchoring conditions on R_1^0, and x axis alignment conditions on R_2^0 [SM Eq. (S29) [60]]. We obtain an active stress distribution given by

$$\nabla \cdot \mathbf{Q}^0 = -[G_2(r)\sin(2\theta) + G_4(r)\sin(4\theta)]\hat{\mathbf{e}}_\theta + [G_0(r) + G_2(r)\cos(2\theta) + G_4(r)\cos(4\theta)]\hat{\mathbf{e}}_r. \tag{9}$$

See SM [60] for the expressions for $G_i(r, \Lambda)$. We point out the presence of $n = 0$, 2, and 4 modes in the driving force appearing in the Stokes equation at $\mathcal{O}(\epsilon_\alpha)$, which will drive the free surfaces away from circular. Figure 2(a) illustrates the nematic texture and active driving surrounding the wound free boundary. We also highlight the presence of two $-\frac{1}{2}$ topological defects [54–58,67] in the alignment field, which, as the wound closes, move toward its center. Since the wound itself provides an additional $+1$ topological charge, upon closure, the tissue returns to a topologically neutral healed state. An illustration of the defect motion during closure is illustrated in Fig. 2(b).

Activity drives closure and noncircular wound shapes—To compactly express the flow at $\mathcal{O}(\epsilon_\alpha)$, it is convenient to use the stream function $\mathbf{v}^1 = \nabla \times (\psi^1 \hat{\mathbf{e}}_z)$ of the velocity field. Taking the curl of the Stokes equation at $\mathcal{O}(\epsilon_\alpha)$, the stream function satisfies a driven, modified biharmonic equation,

$$\nabla^4 \psi^1 - \nabla^2 \psi^1 = F_2(r, \Lambda)\sin 2\theta + F_4(r, \Lambda)\sin 4\theta. \tag{10}$$

See SM [60] for the expressions for $F_i(r, \Lambda)$. After solving for the p^1, $\mathbf{v}^1$ [68], the kinematic boundary condition provide a series of ODEs for the dynamics of shape mode amplitudes, $\dot{\xi}_i^n, \dot{\eta}_i^n$, $n = 0$, 2, 4 [see Eq. (7) and SM Eq. (S36) [60]]. Crucially, we observe that the circular (ξ_i^0) and quadropolar ($\xi_i^{2,4}$) modes are driven, arising from the active forces in the bulk [Eq. (9)]. Numerically

integrating these ODEs (SM Fig. S2 [60]) determines the boundary shapes and solves the problem.

Hence we find that stresses of the form $\sim\alpha\mathbf{Q}$ drive the wound (free surface) away from circular [Fig. 2(c)], the degree of anisotropy increasing with ϵ_α and elongating parallel (perpendicular) to the x axis in the contractile, $\epsilon_\alpha > 0$ (extensile, $\epsilon_\alpha < 0$), case. This prediction is validated by our experimental observations: plotting the degree of nematic order in the tissue, $\langle\|q_{\text{tissue}}\|\rangle$ against the anisotropy of the wound polygon, $\langle\|q_{\text{wound}}\|\rangle$ indicates that samples with stronger nematic ordering in the bulk are those with greater anisotropy in the wound shape [Fig. 2(e)]. Stronger nematic order also implies a smaller nematic length: $\ell_Q \sim 1/\sqrt{Q_0}$ (see SM [60]). Further, by measuring the angle between the tissue axis and the wound's major axis for each sample, θ_{w} [Fig. 2(e) and SM [60]) we find that wounds tend to elongate *parallel* to the tissue axis (see SM [60] for details). Elongation along the tissue axis is a signature of *contractility* in our model [Fig. 2(c)], suggesting the surrounding tissue is under contractile stress. This is consistent with another prediction of our model, namely that contractility ($\epsilon_\alpha > 0$) *accelerates* closure, while extensility ($\epsilon_\alpha < 0$) *delays* it [Fig. 2(c)]. This is a consequence of the parallel anchoring conditions on $\mathbf{Q}$, *observed experimentally*, at the wound free surface; normal anchoring at the wound edge interchanges the effects of contractility or extensility on rates of closure (see SM Fig. S6 [60]).

Conclusion and discussion—Informed by experimental observations of reepithelialization, we have solved the free-boundary problem of a closing hole in an active nematic tissue. We find that for parallel-anchored nematic alignment at the wound hole, contractile active stresses in the bulk tissue (a) accelerate healing and (b) drive elongation of the wound along the axis of bulk nematic order. Our model suggests the tissue in our experiments is under a state of contractile active stress—a prediction that is supported by our measurements of wound anisotropy and alignment parallel to the axis of nematic order in the surrounding tissue.

We have taken the alignment conditions at the boundaries as inputs to the model, i.e., we do not explain what causes the parallel anchoring in our experiments nor do we allow for dynamics in this nematic order. The precise nature of the mechanism that causes specific cellular alignments at epithelial gaps is the subject of ongoing research [69]. However, given that we observe tangential cellular alignment on a timescale shorter (~5–10 min) than the timescale for formation of the actin purse string (reported as ~15–30 min for wounds in the notum epithelium of *Drosophila* at a similar stage of development [39]), it is likely that the passive release of mechanical tension and recoil following wounding is relevant.

Although we have focused on reepithelialization of wounds in *Drosophila* pupae, this Letter highlights the relevance of tissue structure and bulk force generation in epithelial gaps more generally [70]. It would be interesting to see how these ideas extend to understanding the mechanics of epithelial closure events in other biological contexts; for example *Ciona* neural tube closure [71] or *Drosophila* dorsal closure [72], where cells tend to align perpendicular to the epithelial gap boundaries instead.

Acknowledgments—T. B. L., J. T., I. V. C., R. R. B., and H. A. would like to thank the Isaac Newton Institute for Mathematical Sciences, Cambridge, for support and hospitality during the program "New statistical physics in living matter," where part of this work was done. This work was supported by EPSRC Grants No. EP/R014604/1 and No. EP/T031077/1. H. A. acknowledges the support of an EPSRC studentship and thanks Luke Neville for helpful discussions and advice regarding calculational details. J. T. is supported by the Eric and Wendy Schmidt AI in Science Postdoctoral Fellowship. We acknowledge the facilities of the Advanced Computing Research Centre, Bristol University.

Data availability—The data that support the findings of this article are openly available [68]; embargo periods may apply.

[1] C. Collinet and T. Lecuit, Programmed and self-organized flow of information during morphogenesis, Nat. Rev. Mol. Cell Biol. **22**, 245 (2021).
[2] G. C. Gurtner, S. Werner, Y. Barrandon, and M. T. Longaker, Wound repair and regeneration, Nature (London) **453**, 314 (2008).
[3] S. A. Eming, P. Martin, and M. Tomic-Canic, Wound repair and regeneration: Mechanisms, signaling, and translation, Sci. Transl. Med. **6**, 265sr6 (2014).
[4] O. A. Peña and P. Martin, Cellular and molecular mechanisms of skin wound healing, Nat. Rev. Mol. Cell Biol. **25**, 599 (2024).
[5] K. E. Degen and R. G. Gourdie, Embryonic wound healing: A primer for engineering novel therapies for tissue repair, Birth Defects Res. Part C **96**, 258 (2012).
[6] P. Martin and R. Nunan, Cellular and molecular mechanisms of repair in acute and chronic wound healing, Br. J. Dermatol. **173**, 370 (2015).
[7] S. Park, D. G. Gonzalez, B. Guirao, J. D. Boucher, K. Cockburn, E. D. Marsh, K. R. Mesa, S. Brown, P. Rompolas, A. M. Haberman, Y. Bellaïche, and V. Greco, Tissue-scale coordination of cellular behaviour promotes epidermal wound repair in live mice, Nat. Cell Biol. **19**, 155 (2017).
[8] M. Aragona, S. Dekoninck, S. Rulands, S. Lenglez, G. Mascré, B. D. Simons, and C. Blanpain, Defining stem cell dynamics and migration during wound healing in mouse skin epidermis, Nat. Commun. **8**, 14684 (2017).
[9] W. Razzell, W. Wood, and P. Martin, Recapitulation of morphogenetic cell shape changes enables wound re-epithelialisation, Development **141**, 1814 (2014).

[10] R. J. Tetley, M. F. Staddon, D. Heller, A. Hoppe, S. Banerjee, and Y. Mao, Tissue fluidity promotes epithelial wound healing, Nat. Phys. **15**, 1195 (2019).
[11] J. Turley, F. Robertson, I. V. Chenchiah, T. B. Liverpool, H. Weavers, and P. Martin, Deep learning reveals a damage signalling hierarchy that coordinates different cell behaviours driving wound re-epithelialisation, Development **151**, dev202943 (2024).
[12] B. Garcia-Fernandez, I. Campos, J. Geiger, A. C. Santos, and A. Jacinto, Epithelial resealing, Int. J. Dev. Biol. **53**, 1549 (2009).
[13] W. Wood, A. Jacinto, R. Grose, S. Woolner, J. Gale, C. Wilson, and P. Martin, Wound healing recapitulates morphogenesis in *Drosophila* embryos, Nat. Cell Biol. **4**, 907 (2002).
[14] M. J. Galko and M. A. Krasnow, Cellular and genetic analysis of wound healing in *Drosophila* larvae, PLoS Biol. **2**, e239 (2004).
[15] H. Weavers, J. Liepe, A. Sim, W. Wood, P. Martin, and M. P. H. Stumpf, Systems analysis of the dynamic inflammatory response to tissue damage reveals spatiotemporal properties of the wound attractant gradient, Curr. Biol. **26**, 1975 (2016).
[16] M. Rämet, R. Lanot, D. Zachary, and P. Manfruelli, JNK signaling pathway is required for efficient wound healing in *Drosophila*, Dev. Biol. **241**, 145 (2002).
[17] A. Franz, W. Wood, and P. Martin, Fat body cells are motile and actively migrate to wounds to drive repair and prevent infection, Dev. Cell **44**, 460 (2018).
[18] J. McCluskey, J. Hopkinson-Woolley, B. Luke, and P. Martin, A study of wound healing in the E11.5 mouse embryo by light and electron microscopy, Tissue Cell **25**, 173 (1993).
[19] W. Razzell, W. Wood, and P. Martin, Swatting flies: Modelling wound healing and inflammation in *Drosophila*, Dis. Models Mech. **4**, 569 (2011).
[20] V. Muñoz-Soriano, S. López-Domenech, and N. Paricio, Why mammalian wound-healing researchers may wish to turn to *Drosophila* as a model, Exp. Dermatol. **23**, 538 (2014).
[21] J. Turley, I. V. Chenchiah, T. B. Liverpool, H. Weavers, and P. Martin, What good is maths in studies of wound healing?, iScience **25**, 104778 (2022).
[22] K. J. Sonnemann and W. M. Bement, Wound repair: Toward understanding and integration of single-cell and multicellular wound responses, Annu. Rev. Cell Dev. Biol. **27**, 237 (2011).
[23] J. C. Arciero, Q. Mi, M. F. Branca, D. J. Hackam, and D. Swigon, Continuum model of collective cell migration in wound healing and colony expansion, Biophys. J. **100**, 535 (2011).
[24] L. G. Bowden, H. M. Byrne, P. K. Maini, and D. E. Moulton, A morphoelastic model for dermal wound closure, Biomech. Model. Mechanobiol. **15**, 663 (2016).
[25] M. Poujade, E. Grasland-Mongrain, A. Hertzog, J. Jouanneau, P. Chavrier, B. Ladoux, A. Buguin, and P. Silberzan, Collective migration of an epithelial monolayer in response to a model wound, Proc. Natl. Acad. Sci. U.S.A. **104**, 15988 (2007).
[26] O. Cochet-Escartin, J. Ranft, P. Silberzan, and P. Marcq, Border forces and friction control epithelial closure dynamics, Biophys. J. **106**, 65 (2014).
[27] L. Almeida, P. Bagnerini, and A. Habbal, Modeling actin cable contraction, Comput. Math. Appl. **64**, 310 (2012).
[28] A. Ravasio, I. Cheddadi, T. Chen, T. Pereira, H. T. Ong, C. Bertocchi, A. Brugues, A. Jacinto, A. J. Kabla, Y. Toyama, X. Trepat, N. Gov, L. Neves de Almeida, and B. Ladoux, Gap geometry dictates epithelial closure efficiency, Nat. Commun. **6**, 7683 (2015).
[29] X. Chen and A. Friedman, A free boundary problem arising in a model of wound healing, SIAM J. Math. Anal. **32**, 778 (2000).
[30] C. Xue, A. Friedman, and C. K. Sen, A mathematical model of ischemic cutaneous wounds, Proc. Natl. Acad. Sci. U.S.A. **106**, 16782 (2009).
[31] S. Mark, R. Shlomovitz, N. S. Gov, M. Poujade, E. Grasland-Mongrain, and P. Silberzan, Physical model of the dynamic instability in an expanding cell culture, Biophys. J. **98**, 361 (2010).
[32] L. Roldán, J. J. Muñoz, and P. Sáez, Computational modeling of epithelial wound healing: Short and long term chemo-mechanical mechanisms, Comput. Methods Appl. Mech. Eng. **350**, 28 (2019).
[33] P. Martin and J. Lewis, Actin cables and epidermal movement in embryonic wound healing, Nature (London) **360**, 179 (1992).
[34] Z. Kamran, K. Zellner, H. Kyriazes, C. M. Kraus, J.-B. Reynier, and J. E. Malamy, In vivo imaging of epithelial wound healing in the cnidarian Clytia hemisphaerica demonstrates early evolution of purse string and cell crawling closure mechanisms, BMC Dev. Biol. **17**, 17 (2017).
[35] M. Tamada, T. D. Perez, W. J. Nelson, and M. P. Sheetz, Two distinct modes of myosin assembly and dynamics during epithelial wound closure, J. Cell Biol. **176**, 27 (2007).
[36] P. Martin, C. Nobes, J. McCluskey, and J. Lewis, Repair of excisional wounds in the embryo, Eye **8**, 155 (1994).
[37] A. Brugués, E. Anon, V. Conte, J. H. Veldhuis, M. Gupta, J. Colombelli, J. J. Muñoz, G. W. Brodland, B. Ladoux, and X. Trepat, Forces driving epithelial wound healing, Nat. Phys. **10**, 683 (2014).
[38] Y. Matsubayashi, W. Razzell, and P. Martin, "White wave" analysis of epithelial scratch wound healing reveals how cells mobilise back from the leading edge in a myosin-II-dependent fashion, J. Cell Sci. **124**, 1017 (2011).
[39] M. Antunes, T. Pereira, J. V. Cordeiro, L. Almeida, and A. Jacinto, Coordinated waves of actomyosin flow and apical cell constriction immediately after wounding, J. Cell Biol. **202**, 365 (2013).
[40] P. Lee and C. W. Wolgemuth, Crawling cells can close wounds without purse strings or signaling, PLoS Comput. Biol. **7**, e1002007 (2011).
[41] S. C. Kammeraat *et al.*, Correlated cell movements drive epithelial finger formation, arXiv:2508.01046.
[42] C. Villeneuve, K. P. McCreery, and S. A. Wickström, Measuring and manipulating mechanical forces during development, Nat. Cell Biol. **27**, 575 (2025).

[43] B. Ladoux and R.-M. Mège, Mechanobiology of collective cell behaviours, Nat. Rev. Mol. Cell Biol. **18**, 743 (2017).
[44] R. Etournay, M. Popović, M. Merkel, A. Nandi, C. Blasse, B. Aigouy, H. Brandl, G. Myers, G. Salbreux, F. Jülicher, and S. Eaton, Interplay of cell dynamics and epithelial tension during morphogenesis of the *Drosophila* pupal wing, eLife **4**, e07090 (2015).
[45] J. Comelles, S. SS, L. Lu, E. Le Maout, S. Anvitha, G. Salbreux, F. Jülicher, M. M. Inamdar, and D. Riveline, Epithelial colonies *in vitro* elongate through collective effects, eLife **10**, e57730 (2021).
[46] E.-M. Schötz, M. Lanio, J. A. Talbot, and M. L. Manning, Glassy dynamics in three-dimensional embryonic tissues, J. R. Soc. Interface **10**, 20130726 (2013).
[47] M. Olenik, J. Turley, S. Cross, H. Weavers, P. Martin, I. V. Chenchiah, and T. B. Liverpool, Fluctuations of cell geometry and their nonequilibrium thermodynamics in living epithelial tissue, Phys. Rev. E **107**, 014403 (2023).
[48] J. Turley, I. V. Chenchiah, P. Martin, T. B. Liverpool, and H. Weavers, Deep learning for rapid analysis of cell divisions *in vivo* during epithelial morphogenesis and repair, eLife **12**, RP87949 (2024).
[49] J. Turley, Deep learning and mathematical analysis of wound healing in flies; Live imaging in *Drosophila*, Ph.D. thesis, University of Bristol, 2023.
[50] T. B. Saw, W. Xi, B. Ladoux, and C. T. Lim, Biological tissues as active nematic liquid crystals, Adv. Mater. **30**, 1802579 (2018).
[51] A. Doostmohammadi, J. Ignés-Mullol, J. M. Yeomans, and F. Sagués, Active nematics, Nat. Commun. **9**, 3246 (2018).
[52] S. Ramaswamy, The mechanics and statistics of active matter, Annu. Rev. Condens. Matter Phys. **1**, 323 (2010).
[53] M. C. Marchetti, J. F. Joanny, S. Ramaswamy, T. B. Liverpool, J. Prost, M. Rao, and R. A. Simha, Hydrodynamics of soft active matter, Rev. Mod. Phys. **85**, 1143 (2013).
[54] D. Dell'Arciprete, M. L. Blow, A. T. Brown, F. D. C. Farrell, J. S. Lintuvuori, A. F. McVey, D. Marenduzzo, and W. C. K. Poon, A growing bacterial colony in two dimensions as an active nematic, Nat. Commun. **9**, 4190 (2018).
[55] L. A. Hoffmann, L. N. Carenza, J. Eckert, and L. Giomi, Theory of defect-mediated morphogenesis, Sci. Adv. **8**, eabk2712 (2022).
[56] K. Kawaguchi, R. Kageyama, and M. Sano, Topological defects control collective dynamics in neural progenitor cell cultures, Nature (London) **545**, 327 (2017).
[57] Y. Maroudas-Sacks, L. Garion, L. Shani-Zerbib, A. Livshits, E. Braun, and K. Keren, Topological defects in the nematic order of actin fibres as organization centres of Hydra morphogenesis, Nat. Phys. **17**, 251 (2021).
[58] T. B. Saw, A. Doostmohammadi, V. Nier, L. Kocgozlu, S. Thampi, Y. Toyama, P. Marcq, C. T. Lim, J. M. Yeomans, and B. Ladoux, Topological defects in epithelia govern cell death and extrusion, Nature (London) **544**, 212 (2017).
[59] P. G. de Gennes, Short range order effects in the isotropic phase of nematics and cholesterics, Mol. Cryst. Liq. Cryst. **12**, 193 (1971).
[60] See Supplemental Material at http://link.aps.org/supplemental/10.1103/8871-8m6c for further calculational details and links to *Mathematica* code used to solve this problem.
[61] P. M. Chaikin and T. C. Lubensky, *Principles of Condensed Matter Physics* (Cambridge University Press, Cambridge, England, 1995), 10.1017/CBO9780511813467.
[62] A. N. Beris and B. J. Edwards, *Thermodynamics of Flowing Systems: With Internal Microstructure* (Oxford University Press, New York, 1994).
[63] M. E. Cates and E. Tjhung, Theories of binary fluid mixtures: From phase-separation kinetics to active emulsions, J. Fluid Mech. **836**, P1 (2018).
[64] R. A. Simha and S. Ramaswamy, Hydrodynamic fluctuations and instabilities in ordered suspensions of self-propelled particles, Phys. Rev. Lett. **89**, 058101 (2002).
[65] G. K. Batchelor, *An Introduction to Fluid Dynamics*, Cambridge Mathematical Library (Cambridge University Press, Cambridge, England, 2000).
[66] R. Alert, Fingering instability of active nematic droplets, J. Phys. A **55**, 234009 (2022).
[67] K. Copenhagen, R. Alert, N. S. Wingreen, and J. W. Shaevitz, Topological defects promote layer formation in *Myxococcus xanthus* colonies, Nat. Phys. **17**, 211 (2021).
[68] *Mathematica* code used to solve the equations of motion and experimental analysis scripts can be found at https://github.com/haandra/dynamicsOfWoundClosure. Experimental data used in analysis of wound shapes has been previously published in [47] and is available at: Turley *et al.*, Zenodo, https://zenodo.org/records/13819609.
[69] H. Andralojc *et al.* (unpublished).
[70] F. Pérez-Verdugo, E. Maniou, G. L. Galea, and S. Banerjee, Anisotropic cell shape and motion coordinate hindbrain neuropore morphogenesis, bioRxiv (2025), 10.1101/2024.11.21.624679.
[71] H. Hashimoto, F. B. Robin, K. M. Sherrard, and E. M. Munro, Sequential contraction and exchange of apical junctions drives zippering and neural tube closure in a simple chordate, Dev. Cell **32**, 241 (2015).
[72] O. De, C. Rice, T. Zulueta-Coarasa, R. Fernandez-Gonzalez, and R. E. Ward, Septate junction proteins are required for cell shape changes, actomyosin reorganization and cell adhesion during dorsal closure in *Drosophila*, Front. Cell Dev. Biol. **10**, 947444 (2022).